Journal of MATERIALS RESEARCH

Invited Feature Paper
DOI: 10.1557/jmr.2019.404

EARLY CAREER SCHOLARS IN MATERIALS SCIENCE

ANNUAL ISSUE

Controlling neutral and charged excitons in MoS_2 with defects

Kory Burns[1], Anne Marie Z. Tan[2], Adam Gabriel[3], Lin Shao[3], Richard G. Hennig[2], Assel Aitkaliyeva[1,a)]

[1]Department of Materials Science and Engineering, University of Florida, Gainesville, Florida 32611, USA
[2]Department of Materials Science and Engineering, University of Florida, Gainesville, Florida 32611, USA; and Quantum Theory Project, University of Florida, Gainesville, Florida 32611, USA
[3]Department of Nuclear Engineering, Texas A&M University, College Station, Texas 77840, USA
[a)]Address all correspondence to this author. e-mail: aitkaliyeva@mse.ufl.edu
This paper has been selected as an Invited Feature Paper.

Received: 10 October 2019; accepted: 13 December 2019

In this contribution, we use heavy ion irradiation and photoluminescence (PL) spectroscopy to demonstrate that defects can be used to tailor the optical properties of two-dimensional molybdenum disulfide (MoS_2). Sonicated MoS_2 flakes were deposited onto Si/SiO_2 substrate and subjected to 3 MeV Au^{2+} ion irradiation at room temperature to fluences ranging from 1×10^{12} to 1×10^{16} cm^{-2}. We demonstrate that irradiation-induced defects can control optical excitations in the inner core shell of MoS_2 by binding A_{1s}- and B_{1s}-excitons, and correlate the exciton peaks to the specific defects introduced with irradiation. The systematic increase of ion fluence produced different defect densities in MoS_2, which were estimated using B/A exciton ratios and progressively increased with ion fluence. We show that up to the fluences of 1×10^{14} cm^{-2}, the MoS_2 lattice remains crystalline and defect densities can be controlled, whereas at higher fluences ($\geq 1 \times 10^{15}$ cm^{-2}), the large number of introduced defects distorts the excitonic structure of the material. In addition to controlling excitons, defects were used to split bound and free trions, and we demonstrate that at higher fluences (1×10^{15} cm^{-2}), both free and bound trions can be observed in the same PL spectrum. Most importantly, the lifetimes of these states exceed trion and exciton lifetimes in pristine MoS_2, and PL spectra of irradiated MoS_2 remains unchanged weeks after irradiation experiments. Thus, this work demonstrated the feasibility of engineering novel optical behaviors in low-dimensional materials using heavy ion irradiation. The insights gained from this study will aid in understanding the many-body interactions in low-dimensional materials and may ultimately be used to develop novel materials for optoelectronic applications.



Assel Aitkaliyeva

Assel Aitkaliyeva is an Assistant Professor of Nuclear Engineering in the Department of Materials Science and Engineering at the University of Florida. She received her Ph.D. in Materials Science & Engineering (2012) and M.S. in Nuclear Engineering (2009) at the Texas A&M University, while working on irradiation stability of low dimensional carbon systems such as nanotubes and graphene. Before joining UF in February 2017, she had postdoc and staff scientist appointments at Idaho National Laboratory (INL). She is the recipient of INL Early Career (2015), US Department of Energy (DOE) Fuel Cycle Research and Development (FCRD) Excellence (2016), and DOE Early Career Awards (2018). Her current research interests include nuclear fuels, with emphasis on characterization and property evaluation; mechanical properties of structural materials; radiation response of materials and fuels; and two-dimensional materials and their stability in extreme environments.

Introduction

Optoelectronic properties of transition metal dichalcogenides (TMDs) can be manipulated by taking the system out of equilibrium, which has been done using temperature [1, 2, 3, 4], pressure [5, 6], electrical bias [7, 8], magnetic fields [9], and light ion [10, 11, 12] and electron irradiations [12, 13].

© Materials Research Society 2020. This is an Open Access article, distributed under the terms of the Creative Commons Attribution licence (http://creativecommons.org/licenses/by/4.0/), which permits unrestricted re-use, distribution, and reproduction in any medium, provided the original work is properly cited.

https://doi.org/10.1557/jmr.2019.404 Published online by Cambridge University Press

Molybdenum disulfide (MoS_2) remains the most widely studied TMD material system because of its remarkable flexibility [14] and enhanced photoresponsivity [15]. Fabrication of MoS_2 by chemical vapor deposition (CVD), mechanical exfoliation, and physical vapor deposition introduces intrinsic defects, which has been shown to degrade material's properties [16]. Carbon and oxygen impurities introduced at various stages of fabrication can occupy interstitial sites in MoS_2 [17], act as traps for charge carriers [18], and degrade carrier concentrations [19].

Theory, on the other hand, predicts that defects can be used to control properties of single- and multi-layered materials. According to first principles calculations, native defects such as S and Mo vacancies create impurity levels in bulk MoS_2 within the band gap and in the valence band and lead to pronounced photon absorption in visible light region [20]. These impurity levels can be used to manipulate photovoltaic energy conversion at longer wavelength [20]. Several groups investigated the role defects (mostly vacancies and grain boundaries) play in determining the electronic, optical, and optoelectronic properties of low-dimensional MoS_2 systems, but no explicit understanding of the phenomena has been attained [16, 20, 21, 22, 23, 24]. Most studies focused on doping MoS_2 to achieve control of the optical properties, which included studies on chemical doping [25] and low-energy ion implantation [26].

Instead of concentrating on low-energy ion implantation, we explore intermediate energy ion irradiation to control defect densities in MoS_2. Although low-energy (typically <1 keV) ion implantation provides an exciting route to alter material properties, nuclear energy deposition induces defects that can dominate the material response. In the case of intermediate energies (range from a few hundred keV to several MeV), electronic energy deposition starts to play an important role in the modification of optical properties of these low-dimensional materials. We use ion irradiation to controllably introduce defects and investigate the change in photoluminescence (PL) spectra of MoS_2 and elucidate the role defects play in controlling the optical response of the material.

Results and discussion

Photoexcitation in semiconducting MoS_2 is expected to produce pairs of bound electrons and holes known as excitons, the recombination of which emits a photon observed as PL. Photogenerated electron–hole pairs can have strong Coulomb interaction, leading to the formation of bound excitons, and can alter the optical transitions in these systems. The spatial confinement combined with the reduced dielectric screening as compared with bulk crystals suggests that the optical response of low-dimensional MoS_2 flakes will be dominated by neutral excitons.

Previous studies [27, 28, 29] indicated that the spectrum of bare MoS_2 should display two distinctive peaks: A_{1s} exciton peak between 1.86 and 1.92 eV and B_{1s} exciton peak within the range of 2.0–2.1 eV, which are associated with direct optical transitions to the lowest conduction bands from the highest spin-orbit valence bands [30, 31, 32]. It should be noted that both A_{1s} and B_{1s} exciton peaks are formed by an electron and a hole in the valence band. The ground state A_{1s} exciton has a smaller PL energy than the B_{1s} exciton, which is associated with the spin orbit split valence band. Other possible spectral features in MoS_2 include the A^- trion peak arising from interactions between two electrons and a hole that can occur when excess electrons bind to photoexcited electron–hole pairs and create positively charged states [28, 29, 30]. Previously, optical response of TMDs has been changed using applied bias and femtosecond light pulses that introduced large number of carriers and increased screening of the Coulomb interaction [7, 33]. Generally, using p-type dopants caused a shift toward higher energies in excitonic peaks, whereas n-type dopant caused a shift toward lower energies in excitonic peaks [34, 35].

As seen from Fig. 1, the PL spectrum of the unirradiated sample exhibits an A_{1s} exciton peak at 1.91 eV and a B_{1s} exciton peak at 2.09 eV. The inset in the right bottom corner is a schematic representation of the electron and hole with respect to the Fermi level (E_F) in an exciton. The spectral position of the peak shifts on irradiation and opposing trends were noted for the A_{1s} and B_{1s} exciton peaks: The A_{1s} exciton peak shifts toward higher energies, whereas B_{1s} toward lower energies with increasing ion fluence. Note that Fig. 1 discusses only exciton peaks, and data corresponding to the trion peak will be provided later in the manuscript.

As illustrated in Fig. 1, ion fluence was systematically increased for each consecutive sample to induce higher densities of defects. It should be noted that because MoS_2 specimens were prepared via exfoliation means, the thickness of individual flakes varied from 0.85 nm (mono-layer) to 2.33 nm (tri-layer). These values were experimentally measured using atomic force microscopy before and after irradiation. Understanding that flake thickness might have an impact on the defect densities in the sample, authors performed more than ten measurements for each irradiated specimen at random locations. Based on these measurements, the PL response of MoS_2 is not influenced by thickness of the flakes after ion irradiation but is rather governed by the defects introduced during irradiation. If the thickness of individual flakes altered the position of A excitons, we would have observed variation in positions of the peaks in PL spectra. The data shown in Fig. 1 were representative of the response of the entire irradiated specimen and include data for flakes with varying thicknesses.

The underlying mechanisms governing doping and irradiation are different. Based on our density-functional theory

https://doi.org/10.1557/jmr.2019.404 Published online by Cambridge University Press

© Materials Research Society 2020

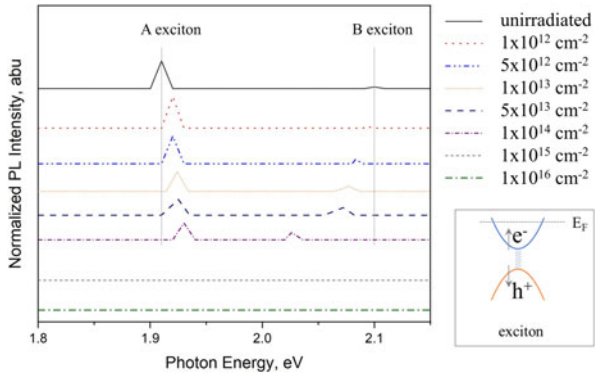


Figure 1: PL of unirradiated MoS_2 specimens and those irradiated to various fluences with 3 MeV Au ions. Here, the peak appearing around 1.91 eV corresponds to A excitons and peak around 2.09 eV to B excitons. The vertical lines are provided for reader's convenience to illustrate the shift in peaks as a function of increasing ion fluence. The inset is a schematic representation of the location of electron and hole in respect to the Fermi energy level in exciton.

(DFT) calculations, the binding energy of Au atom/ion on the surface of MoS_2 is in the range of 0.5–1.0 eV, which is consistent with the values reported in the literature [36, 37]. The binding energy for Au ions are much smaller than the kinetic energy of the impinging Au ions (3 MeV) used in this study, and thus binding of Au ions to the sample and doping is not likely. Instead of doping, energetic Au ions transfer energy to the material and initiate the displacement of atoms from their lattice sites. Ballistic collisions between Au ions and target atoms (Mo and S) lead to the formation of damage cascades that break the periodicity of the lattice. Inelastic collisions excite electrons, ionize target atoms, and result in short-lived electronic excitations.

Irradiation can produce various defect configurations in low-dimensional MoS_2, including vacancies, adatoms, vacancy clusters, grain boundaries with complex dislocation cores, and interfaces with lattice mismatch. DFT calculations indicate that vacancies and vacancy clusters are the most abundant point defect type in MoS_2, which can include single sulfur vacancy (V_s) and double sulfur vacancy (V_{s2}), alongside less energetically favorable antisite defects where Mo occupies V_{s2} (Mo_{S2}), and a pair of S atoms occupying Mo position (S_{2Mo}) [38].

The number of introduced defects is expected to progressively increase with increasing ion fluence. At higher ion fluences ($\geq 1 \times 10^{15}$ cm^{-2}), the accumulated damage eliminates both exciton peaks in MoS_2 as can be seen in Fig. 1. To further illustrate this trend, Fig. 2(a) plots both A_{1s} and B_{1s} exciton peaks as a function of increasing ion fluence. As can be seen from Fig. 2(a), exciton peaks are getting closer, which generally indicates a reduction in the spin-orbit coupling in MoS_2, but additional work is needed to confirm this observation. Figure 2(b) plots the B/A exciton ratios as a function of increasing fluence.

In the past, the B/A exciton ratio has been used to estimate the defect density of pristine MoS_2 flakes. High-quality MoS_2 monolayers grown using CVD method were shown to have B/A ratios between 0.01–0.03 [31]. The B/A ratio of unirradiated MoS_2 used in this study was 0.03, which is comparable to that of CVD grown MoS_2 and indicates good initial sample quality. On irradiation to the lowest fluence of 1×10^{12} cm^{-2}, the B/A ratio doubles (0.06) and reaches 0.52 at the intermediate fluence of 1×10^{14} cm^{-2}. Thus, up to the fluences of 1×10^{14} cm^{-2}, the lattice remains crystalline and defect densities in MoS_2 can be controlled, whereas at higher fluences, large number of introduced defects distorts excitonic structure of the material.

Preliminary DFT calculations were conducted in parallel to our experimental work. Theory indicates that point defects, such as sulfur vacancies, are the most common defect type in MoS_2. The relaxation of the structure is minimal on formation of vacancies, and neutrally charged defects retain trigonal symmetry. DFT calculations of the formation energies of the S vacancy [illustrated in Fig. 3(a)] and S divacancy [shown in Fig. 3(b)] in monolayer MoS_2 in the Mo-rich/S-poor limit are shown in Fig. 3(c) as a function of the Fermi-level position. The valence and conduction band edge positions calculated with respect to the vacuum level are indicated by the vertical dotted lines. The slope of the formation energy plot corresponds to the most stable charge state for the defect over that range of Fermi energies.

The calculated formation energy of the single S vacancy in the Mo-rich/S-poor limit is about 1.25 eV, which is in good agreement with the values reported in the literature [4, 24, 39, 40]. The S vacancy formation energy in the S-rich limit is higher, about 3 eV, but even under those conditions it is still predicted to be one of the lowest energy intrinsic point defects. The formation energy of the S divacancy in the Mo-rich/S-poor limit is calculated to be about 2.4 eV, indicating only a slight binding energy between S vacancies. Our calculations predict that both 0/−1 charge transition levels (CTLs) fall within the band gap and are about 1.55–1.65 eV above the valence band minimum (VBM) in monolayer MoS_2, again in good agreement with other computational studies [4, 24, 39, 41]. The CTLs indicate the presence of (deep acceptor) defect states in the gap which could trap excitons.

Experimentally, we observe a sharp peak at ~1.82 eV in the PL spectra of the sample irradiated to 1×10^{16} cm^{-2} [see Fig. 4(a)] and ~1.70 eV in the sample irradiated to 1×10^{15} cm^{-2} [see Fig. 4(b)]. These peaks were not observed in samples irradiated to lower fluences and are believed to arise from the valley excitons migrating to defects such as sulfur vacancies, which are formed in higher concentrations under higher irradiation fluences. Excitons have been known to migrate to defect bound states in monolayer MoS_2, and the

https://doi.org/10.1557/jmr.2019.404 Published online by Cambridge University Press

© Materials Research Society 2020

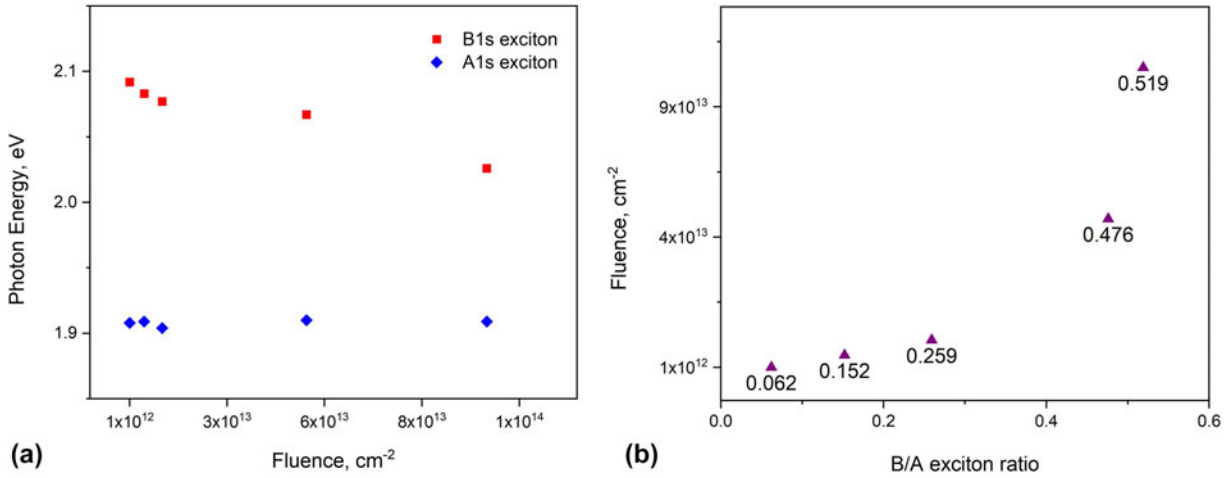


Figure 2: Relationship between A and B exciton peaks and ion fluence in irradiated MoS_2 samples, where (a) plots A_{1s} and B_{1s} exciton peak energies as a function of increasing ion fluence and (b) illustrates how B/A exciton ratios change with ion fluence.

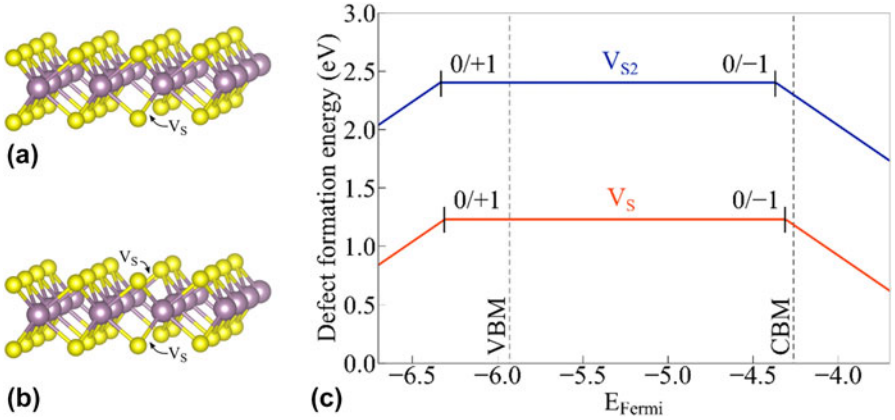


Figure 3: DFT simulation results showing schematics of (a) S vacancy V_s and (b) S divacancy V_{s2}, where Mo atoms are shown in purple and S in yellow, and (c) formation energies of V_s and V_{s2} in monolayer MoS_2 in the Mo-rich/S-poor limit, as a function of Fermi level position. For both defects, the 0/−1 CTL is predicted to be within the band gap and to be associated with a defect level close to the conduction band minimum.

PL peaks (at 1.70 and 1.82 eV) have been previously verified to be reflective of a defect bound state [41, 42, 43]. With DFT predicting that V_s and V_{s2} are the most favorable defect types that form in MoS_2, it is likely that the observed PL peaks are associated with these defects. DFT predicts that the defect states introduced by S vacancies and divacancies are toward the top of the band gap, which is consistent with the energies of the observed PL peaks. However, more detailed calculations at higher level of theory are needed to obtain a better quantitative comparison between experiments and theory.

It is possible that the sample irradiated to the highest fluence has amorphized and the observed line could be reflective of the crystalline-to-amorphous transition. While the free-standing specimens irradiated to the same fluence were determined to be crystalline in nature through transmission electron microscopy imaging, specimens on the substrate cannot be examined in the same fashion. Thus, we cannot rule out the possibility of the amorphization of MoS_2 flakes at the highest irradiation fluence due to extensive collision cascades in the substrate that introduce additional damage to MoS_2. Further studies will be conducted to ascertain the crystalline state of the specimen and confirm that the observed peaks indeed correspond to V_s and V_{s2}.

Although initial assessment is promising, more work needs to be performed to match experimental results with theoretical predictions. Theory agrees that the A_{1s} and B_{1s} excitons should be within the energy range determined experimentally in this work. Nonetheless, DFT has limitations such as underestimation of the band gap and not considering exciton binding in these systems. DFT calculations can predict defect formation energies and the effect these defects can have on optical response of the material; they are difficult to match experimentally. For instance, due to the limitations of standard ground state DFT with semi-local functionals, we are unable

https://doi.org/10.1557/jmr.2019.404 Published online by Cambridge University Press

© Materials Research Society 2020

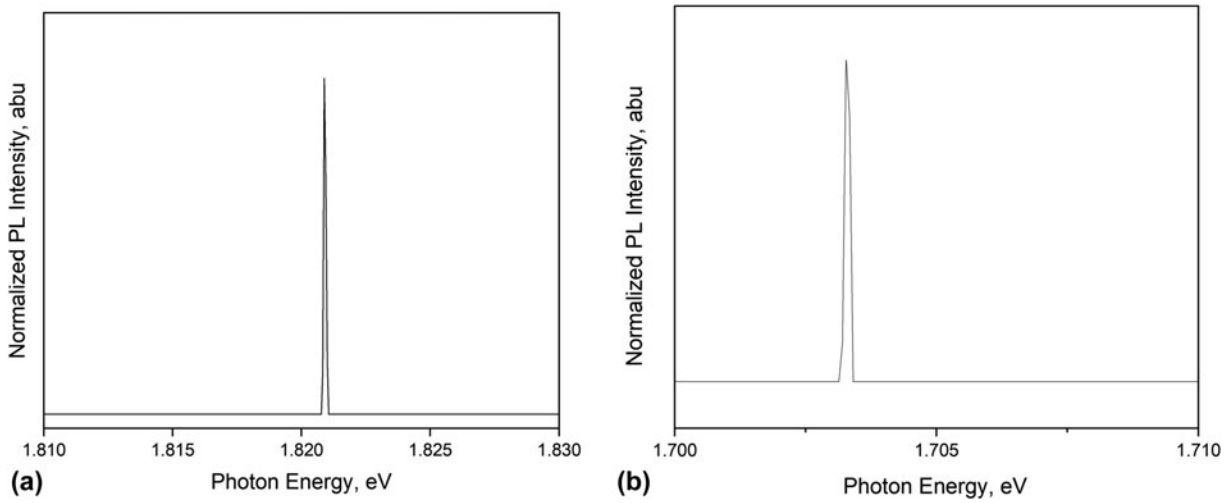


Figure 4: PL peaks observed in samples irradiated with 3 MeV Au ions to fluences of (a) 1×10^{16} cm^{-2} and (b) 1×10^{15} cm^{-2}.

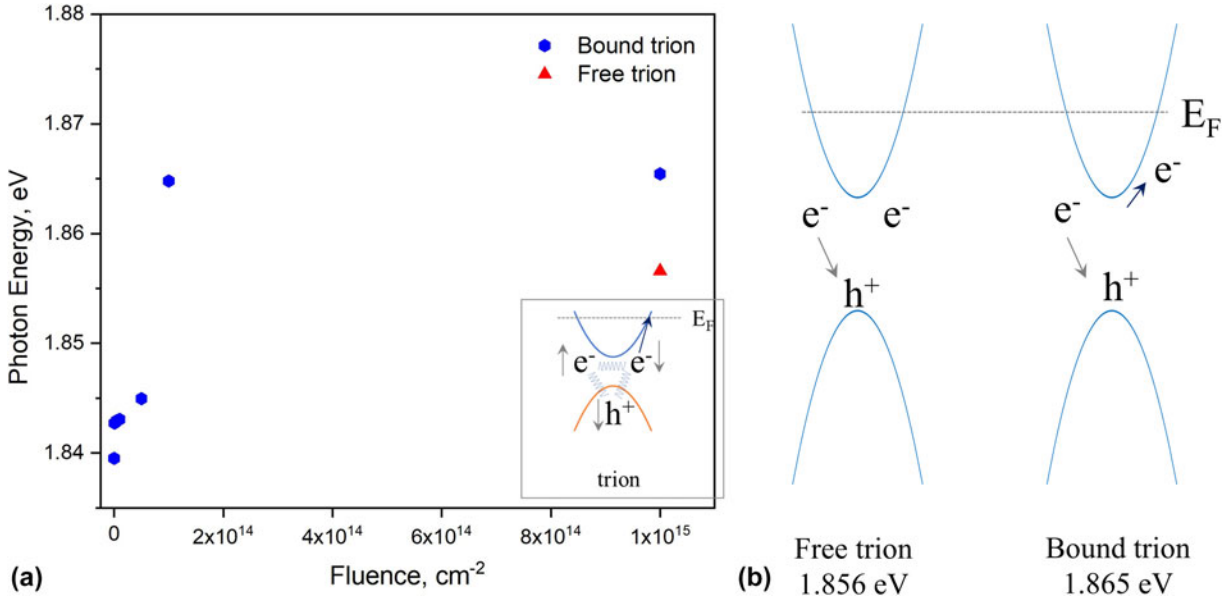


Figure 5: (a) Dependence on ion fluence of the trion peaks and (b) corresponding schematic illustration of the bound and free trions in MoS_2. The inset in (a) is a schematic representation of the location of electrons and a hole in respect to Fermi energy level in trion.

to make quantitative predictions of the energy of such transitions for direct comparison with the experimental results. Therefore, further work needs to be performed to achieve better integration between experiments and modeling.

Beyond controlling neutral excitons, defects can bind photoexcited electron–hole pairs and transfer the exciton spectral weight to trions. We observe the photoemission splitting between bound and free trions, as can be seen from Fig. 5(a), where bound trions are illustrated in blue and the free trion in red. The inset in Fig. 5(a) depicts the position of electrons and holes with respect to E_F in a trion. Figure 5(b) highlights the difference between bound and free trions in MoS_2. In the sample irradiated to the fluence of 1×10^{15} cm^{-2}, both free and bound trions are present within the same PL spectrum. The lifetimes of the states are much longer than the trion/exciton lifetimes, as PL spectra of irradiated MoS_2 samples remains unchanged weeks after irradiation experiments.

It is known that 2H–MoS_2 breaks inversion symmetry in a singular layer but restores it in even number of layers [40, 43]. The lack of inversion symmetry in monolayer MoS_2 (that arises due to the coupling of valley and spin degrees) allows manipulation of the single valley using defects. Furthermore, bulk MoS_2 is an indirect band gap material with a band gap of ~1.2 eV, which transitions to a direct band gap semiconductor with an optical band gap of ~1.87 eV when thinned to its monolayer form [44]. In this study, we did not fabricate

https://doi.org/10.1557/jmr.2019.404 Published online by Cambridge University Press

© Materials Research Society 2020

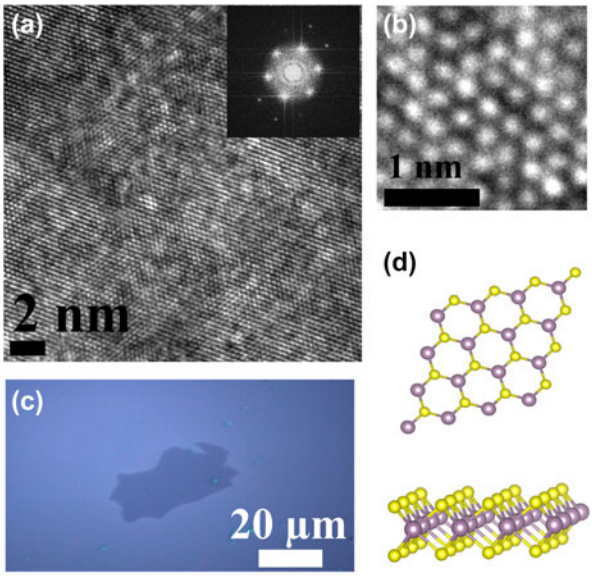


Figure 6: Overview of the MoS_2 samples used in this study: (a) TEM micrograph of the MoS_2 flake, where the inset reflects the 2H phase of the material; (b) high-resolution TEM micrograph of the atomic structure; (c) optical micrograph of large area pristine MoS_2 on Si/SiO_2 substrate; and (d) top view and side view of the atomic structure of monolayer MoS_2, where Mo atoms are depicted in purple and S atoms in yellow.

monolayer MoS_2 and presented data averages over the response of mono-, bi-, and tri-layered flakes, which highlights the versatility of our approach. In the future, the response of mono- and bi-layer flakes to irradiation will be investigated individually to determine if there is a correlation between defect-bound states and number of layers.

Because atomic structure of MoS_2 is trigonal prismatic with hexagonal lattice occupied by one Mo and two S atoms, both highest valence bands and lowest conduction bands of MoS_2 primarily form from Mo *d*-orbitals [45, 46]. Previous theoretical calculations indicated that strongly localized Mo *d*-orbitals are primary contributors to the conduction band states at the *K* point, which have minimal interlayer coupling. However, linear combination of Mo *d*-orbitals with antibonding S p_z-orbitals near the Γ point can lead to strong interlayer coupling. The defects introduced in the course of irradiation can reside between layers and alter *d*-electron physics. Thus, our work demonstrates the feasibility of engineering novel optical behaviors in these materials using defects, which were previously thought to be detrimental to device performance.

Conclusion

In this study, the value of defect engineering in tailoring optical response of low-dimensional MoS_2 flakes was demonstrated. We conducted a systematic study of the scientific phenomena that define optical properties of MoS_2 and attempted to establish a correlation between optical properties and defects. Although previous studies indicate that intrinsic defects and other structural imperfections are not necessarily detrimental to the properties of the material, the role of extrinsic defects in defining the properties of MoS_2 was not clear. We illustrate that irradiation-induced defects provide benefits to optical properties of these two-dimensional materials and can be used to bind excitons and trions to enhance device performance and enable unprecedented functionalities. With the study of structural defects in two-dimensional materials still in its infancy, additional work should be conducted in the future to ensure that the gap between experiments and computational work is bridged and has a sound foundation.

Materials and methods

Experimental details

Molybdenum disulfide ultrafine powder with average particle size of ~90 nm and specific surface area of ~35 m^2/g was purchased from the Graphene Supermarket (Reading, MA). Before irradiation studies, the quality of MoS_2 was ascertained in FEI Tecnai F20 scanning/transmission electron microscope (S/TEM) operated at an accelerating voltage of 80 kV. Figure 6(a) provides a representative overview of an individual MoS_2 flake, with an insert showing its crystallographic structure, consistent with 2H-MoS_2. Figure 6(b) shows a high-resolution micrograph of the MoS_2 atomic structure, which is in good agreement with the structure predicted by DFT calculations provided in Fig. 6(d).

For irradiation studies, MoS_2 powder was placed into a 20 mL vial, submerged in an anhydrous *N*,*N*-dimethylformamide (99.8% purity) from Sigma Aldrich (St. Louis, MO) at a concentration of 20 mg/mL, and sonicated for 3.5 h. After completion of the sonication, flakes were transferred to a Si(001) substrate with 300 nm thickness of SiO_2. Figure 6(c) is a representative example of the flakes that were obtained using this methodology and shows an optical micrograph of large area pristine MoS_2 flake on Si/SiO_2 substrate. Note that the flakes obtained using dispersion/sonication techniques varied in thickness (from 0.85 to 2.33 nm) and contained mono-, bi-, and tri-layers of MoS_2.

Specimens were subjected to 3 MeV Au^{2+} ion irradiation at room temperature using a 1.7 MV General Ionex tandem accelerator. The ion fluence ranged from 1×10^{12} to 1×10^{16} cm^{-2}. The target chamber pressure during the irradiation was at about 6×10^{-8} torr. PL spectroscopy was performed on a Horiba Jobin-Yvon LabRam ARAMIS microRaman with 1800 g/mm grating and a cooled CCD detector. The excitation laser used was 632.8 nm (1.96 eV) HeNe, processed at 298 K (±2 K). The laser power on the sample was about 130 μW, which has been proven to have a good signal-to-noize ratio on monolayer materials [47]. To avoid the local heating effect that

https://doi.org/10.1557/jmr.2019.404 Published online by Cambridge University Press

© Materials Research Society 2020

may be induced by the laser, we used a large density filter (50% transparency), analyzed our sample for any visible damage, and checked the intensities of the peaks in the spectra, as decreasing intensity peaks signify heating damage to the material.

Computational details

We computed defect formation energies using density functional theory (DFT) as implemented in the Vienna ab initio simulation package (VASP) [48]. We performed calculations using projector-augmented wave potentials [48, 49, 50] and treat the exchange-correlation using the Perdew–Burke–Ernzerhof (PBE) [51] generalized gradient approximation functional. A plane wave cutoff energy of 520 eV, and Methfessel–Paxton smearing [52] with smearing energy width of 0.10 eV and Γ-centered Monkhorst–Pack k-point meshes [53] were employed for Brillion zone integration. Defect calculations were performed in a 4 × 4 supercell, with 20 Å vacuum spacing between layers, and a 3 × 3 k-point mesh.

The formation energy $E^{f}[X^{q}]$ of a point defect X with charge q is determined by DFT calculations using a supercell approach following:

$$E^{f}[X^{q}] = E_{tot}[X^{q}] - E_{tot}[\text{pristine}] - \Sigma_i n_i \mu_i + qE_F + E_{corr} \quad ,$$

where $E_{tot}[X^{q}]$ and $E_{tot}[\text{pristine}]$ are the total DFT-derived energies of the supercell containing the defect X and the pristine supercell respectively, n_i is the number of atoms of species i added/removed, μ_i is the corresponding chemical potential of the species, and E_F is the Fermi energy. The final term E_{corr} corrects for the artifacts introduced by treating charged defects in the periodic supercell approach, which was evaluated using the method developed by Freysoldt and Neugebauer [54].

Acknowledgments

The work was supported by the U.S. Department of Energy, Office of Science, Basic Energy Sciences, under Award #DE-SC0019014 "Establishing defect-property relationships for 2D-nanomaterials." RGH and AMZT time was supported by the National Science Foundation under Awards 1748464 and 1539916.

References

1. **A. Molina-Sánchez, M. Palummo, A. Marini, and L. Wirtz**: Temperature-dependent excitonic effects in the optical properties of single-layer MoS_2. *Phys. Rev. B* **93**, 155435 (2016).
2. **Y. Hu, F. Zhang, M. Titze, B. Deng, H. Li, and G.J. Cheng**: Straining effects in MoS_2 monolayer on nanostructured substrates: Temperature-dependent photoluminescence and exciton dynamics. *Nanoscale* **10**, 5717 (2018).
3. **X. Yin, Q. Wang, L. Cao, C.S. Tang, X. Luo, Y. Zheng, L.M. Wong, S.J. Wang, S.Y. Quek, W. Zhang, A. Rusydi, and A.T.S. Wee**: Tunable inverted gap in monolayer quasi-metallic MoS_2 induced by strong charge-lattice coupling. *Nat. Commun.* **8**, 486 (2017).
4. **S. Tongay, J. Suh, C. Ataca, W. Fan, A. Luce, J.S. Kang, J. Liu, C. Ko, R. Raghunathanan, J. Zhou, F. Ogletree, J. Li, J.C. Grossman, and J. Wu**: Defects activated photoluminescence in two-dimensional semiconductors: Interplay between bound, charged, and free excitons. *Sci. Rep.* **3**, 2657 (2013).
5. **A.P. Nayak, S. Bhattacharyya, J. Zhu, J. Liu, X. Wu, T. Pandey, C. Jin, A.K. Singh, D. Akinwande, and J. Lin**: Pressure-induced semiconducting to metallic transition in multilayered molybdenum disulphide. *Nat. Commun.* **5**, 3731 (2014).
6. **X. Dou, K. Ding, D. Jiang, and B. Sun**: Tuning and identification of interband transitions in monolayer and bilayer molybdenum disulfide using hydrostatic pressure. *ACS Nano* **8**, 7458 (2014).
7. **O.L. Sanchez, D. Ovchinnikov, S. Misra, A. Allain, and A. Kis**: Valley polarization by spin injection in a light-emitting van der Waals heterojunction. *Nano Lett.* **16**, 5792 (2016).
8. **J.S. Ross, S. Wu, H. Yu, N.J. Ghimire, A.M. Jones, G. Aivazian, J. Yan, D.G. Mandrus, D. Xiao, W. Yao, and X. Xu**: Electrical control of neutral and charged excitons in a monolayer semiconductor. *Nat. Commun.* **4**, 1474 (2013).
9. **A.V. Stier, K.M. McCreary, B.T. Jonker, J. Kono, and S.A. Crooker**: Exciton diamagnetic shifts and valley Zeeman effects in monolayer WS_2 and MoS_2 to 65 Tesla. *Nat. Commun.* **7**, 10643 (2016).
10. **B. Wang, S. Yang, J. Chen, C. Mann, A. Bushmaker, and S.B. Cronin**: Radiation-induced direct bandgap transition in few-layer MoS_2. *Appl. Phys. Lett.* **111**, 131101 (2017).
11. **J. Shin, K. Cho, T. Kim, J. Pak, J. Kim, W. Lee, J. Kim, S. Chung, W. Hong, and T. Lee**: Dose-dependent effect of proton irradiation on electrical properties of WSe_2 ambipolar field effect transistors. *Nanoscale* **11**, 13961 (2019).
12. **T. Vogl, K. Sripathy, A. Sharma, P. Reddy, J. Sullivan, J.R. Machacek, L. Zhang, F. Karouta, B.C. Buchler, M.W. Doherty, Y. Lu, and P.K. Lam**: Radiation tolerance of two-dimensional material-based devices for space applications. *Nat. Commun.* **10**, 1202 (2019).
13. **W.M. Parkin, A. Balan, L. Liang, P.M. Das, M. Lamparski, C.H. Naylor, J.A. Rodríguez-Manzo, A.T. Charlie Johnson, V. Meunier, and M. Drndić**: Raman shifts in electron-irradiated monolayer MoS_2. *ACS Nano* **10**, 4134 (2016).
14. **E. Singh, P. Singh, K.S. Kim, G.Y. Yeom, and H.S. Nalwa**: Flexible molybdenum disulfide (MoS_2) atomic layers for wearable electronics and optoelectronics. *ACS Appl. Mater. Interfaces* **11**, 11061 (2019).
15. **O. Lopez-Sanchez, D. Lembke, M. Kayci, A. Radenovic, and A. Kis**: Ultrasensitive photodetectors based on MoS_2. *Nat. Nanotechnol.* **8**, 497 (2013).
16. **J. Hong, Z. Hu, M. Probert, K. Li, D. Lv, X. Yang, L. Gu, N. Mao, Q. Feng, L. Xie, J. Zhang, D. Wu, Z. Zhang, C. Jin,**

https://doi.org/10.1557/jmr.2019.404 Published online by Cambridge University Press

© Materials Research Society 2020

W. Ji, X. Zhang, J. Yuan, and Z. Zhang: Exploring atomic defects in molybdenum disulphide monolayers. *Nat. Commun.* **6**, 6293 (2015).

17. **R. Addou, S. McDonnell, D. Barrera, Z. Guo, A. Azcatl, J. Wang, H. Zhu, C.L. Hinkle, M. Quevedo-Lopez, H.N. Alshareef, L. Colombo, J.W.P. Hsu, and R.M. Wallace**: Impurities and electronic property variations of natural MoS_2 crystal surfaces. *ACS Nano* **9**, 9124 (2015).
18. **N. Ma and D. Jena**: Charge scattering and mobility in atomically thin semiconductors. *Phys. Rev. X* **4**, 011043 (2014).
19. **Y. Cai, H. Zhou, G. Zhang, and Y. Zhang**: Modulating carrier density and transport properties of MoS_2 by organic molecular doping and defect engineering. *Chem. Mater.* **28**, 8611 (2016).
20. **A. Kumar Saha and S.M. Yoshiya**: Native point defects in MoS_2 and their influences on optical properties by first principles calculations. *Physica B* **532**, 184 (2018).
21. **Z. Yu, Y. Pan, Y. Shen, Z. Wang, Z.Y. Ong, T. Xu, R. Xin, L. Pan, B. Wang, L. Sun, J. Wang, G. Zhang, Y.W. Zhang, Y.W. Shi, and X. Wang**: Towards intrinsic charge transport in monolayer molybdenum disulfide by defect and interface engineering. *Nat. Commun.* **5**, 5290 (2014).
22. **W. Zhou, X. Zou, S. Najmaei, Z. Liu, Y. Shi, J. Kong, J. Lou, P.M. Ajayan, B.I. Yakobson, and J.C. Idrobo**: Intrinsic structural defects in monolayer molybdenum disulfide. *Nano Lett.* **13**, 2615 (2013).
23. **S. Haldar, H. Vovusha, M.K. Yadav, O. Eriksson, and B. Sanyal**: Systematic study of structural, electronic, and optical properties of atomic-scale defects in the two-dimensional transition metal dichalcogenides MX_2 (M = Mo, W; X = S, Se, Te). *Phys. Rev. B* **92**, 235408 (2015).
24. **H.P. Komsa and A.V. Krasheninnikov**: Native defects in bulk and monolayer MoS_2 from first principles. *Phys. Rev. B* **91**, 125304 (2015).
25. **S. Mouri, Y. Miyachi, and K. Matsuda**: Tunable photoluminescence of monolayer MoS_2 via chemical doping. *Nano Lett.* **13**, 5944 (2013).
26. **A. Nipane, D. Karmakar, N. Kaushik, S. Karande, and S. Lodha**: Few-layer MoS_2 p-type devices enabled by selective doping using low energy phosphorus implantation. *ACS Nano* **10**, 2128 (2016).
27. **K. Mak, K. He, J. Shan, and T.F. Heinz**: Control of valley polarization in monolayer MoS_2 by optical helicity. *Nanotechnol* **7**, 494 (2012).
28. **K. Mak, K. He, C. Lee, G. Lee, J. Hone, T.F. Heinz, and J. Shan**: Tightly bound trions in monolayer MoS_2. *Nat. Mater.* **12**, 207 (2012).
29. **G. Wang, L. Bouet, D. Lagarde, M. Vidal, A. Balocchi, T. Amand, X. Marie, and B. Urbaszek**: Valley dynamics probed through charged and neutral exciton emissions in monolayer WSe_2. *Phys. Rev. B* **90**, 075413 (2014).
30. **S. Sim, J. Park, J. Song, C. In, Y. Lee, H. Kim, and H. Choi**: Exciton dynamics in atomically thin MoS_2: Interexcitonic interaction and broadening kinetics. *Phys. Rev. B* **88**, 075434 (2013).
31. **K.M. McCreary, A.T. Hanbicki, S.V. Sivaram, and B.T. Jonker**: A- and B-exciton photoluminescence intensity ratio as a measure of sample quality for transition metal dichalcogenide monolayers. *APL Mater.* **6**, 111106 (2018).
32. **I. Niehues, A. Blob, T. Stiehm, S.M. Vasconcellos, and R. Bratschitsch**: Interlayer excitons in bilayer MoS_2 under uniaxial tensile strain. *Nanoscale* **11**, 12788 (2019).
33. **E.M. Mannebach, R. Li, K. Duerloo, C. Nyby, P. Zalden, T. Vecchione, F. Ernst, A. Reid, T. Chase, X. Shen, S. Weathersby, C. Hast, R. Hettel, R. Coffee, N. Hartmann, A.R. Fry, Y. Yu, L. Cao, T.F. Heinz, E.J. Reed, H.A. Dürr, X. Wang, and A.M. Lindenberg**: Dynamic structural response and deformations of monolayer MoS_2 visualized by femtosecond electron diffraction. *Nano Lett.* **15**, 6889 (2015).
34. **J. Suh, T.L. Tan, W. Zhao, J. Park, D. Lin, T. Park, J. Kim, C. Jin, N. Saigal, S. Ghosh, Z.M. Wong, Y. Chen, F. Wang, W. Walukiewicz, G. Eda, and J. Wu**: Reconfiguring crystal and electronic structures of MoS_2 by substitutional doping. *Nat. Commun.* **9**, 199 (2018).
35. **M. Zhong, C. Shen, L. Huang, H. Deng, G. Shen, H. Zheng, Z. Wei, and J. Li**: Electronic structure and exciton shifts in Sb-doped MoS_2 monolayer. *npj 2D Mater. Appl.* **3**, 1 (2019).
36. **Y-Y. Lin, D.O. Dumcenco, H-P. Komsa, Y. Niimi, A.V. Krasheninnikov, Y-S. Huang, and K. Suenaga**: Properties of individual dopant atoms in single-layer MoS_2: Atomic structure, migration, and enhanced reactivity. *Adv. Mater.* **26**, 2857 (2014).
37. **D. Chen, X. Zhang, J. Tang, H. Cui, and Y. Li**: Noble metal (Pt or Au)-doped monolayer MoS_2 as a promising adsorbent and gas-sensing material to SO_2, SOF_2, and SO_2F_2: A DFT study. *Appl. Phys. A* **124**, 194 (2018).
38. **Z. Lin, B.R. Carvalho, E. Kahn, R. Lv, R. Rao, H. Terrones, M.A. Pimenta, and M. Terrones**: Defect engineering of two-dimensional transition metal dichalcogenides. *2D Mater.* **3**, 022002 (2016).
39. **M.H. Naik and M. Jain**: Substrate screening effects on the quasiparticle band gap and defect charge transition levels in MoS_2. *Phys. Rev. Mater.* **2**, 084002 (2018).
40. **J-Y. Noh, H. Kim, and Y-S. Kim**: Stability and electronic structures of native defects in single-layer MoS_2. *Phys. Rev. B* **89**, 205417 (2014).
41. **J. Pandey and A. Soni**: Unraveling biexciton and excitonic excited states from defect bound states in monolayer MoS_2. *Appl. Surf. Sci.* **463**, 52 (2019).
42. **N. Saigal and S. Ghosh**: Evidence for two distinct defect related luminescence features in monolayer MoS_2. *Appl. Phys. Lett.* **109**, 122105 (2016).
43. **T. Cao, J. Feng, J. Shi, Q. Niu, and E. Wang**: Valley-sensitive circular dichroism of monolayer molybdenum disulphide. *Nat. Commun.* **3**, 887 (2012).
44. **J. Gusakova, X. Wang, L. Shiau, A.K.V. Shaposhnikov, V. Borisenko, V. Gusakov, and B. Tay**: Electronic properties of bulk

https://doi.org/10.1557/jmr.2019.404 Published online by Cambridge University Press

© Materials Research Society 2020

and monolayer TMDs: Theoretical study within DFT framework (GVJ-2e method). *Phys. Status Solidi A* **214**, 1700218 (2017).

45. **T. Li and G. Galli**: Electronic properties of MoS_2 nanoparticles. *J. Phys. Chem. C* **111**, 16192 (2007).
46. **L. Mattheiss**: Band structures of transition-metal-dichalcogenide layer compounds. *Phys. Rev. B* **8**, 3719 (1973).
47. **O. Burak Aslan, I.M. Datye, M.J. Mleczko, K. Sze Cheung, S. Krylyuk, A. Bruma, I. Kalish, A.V. Davydov, E. Pop, and T.F. Heinz**: Probing the optical properties and strain-tuning of ultrathin $Mo_{1-x}W_xTe_2$. *Nano Lett.* **18**, 2485 (2018).
48. **G. Kresse and J. Furthmüller**: Efficient iterative schemes for ab initio total-energy calculations using a plane-wave basis set. *Phys. Rev. B* **54**, 11169 (1996).
49. **P.E. Blöchl**: Projector augmented-wave method. *Phys. Rev. B* **50**, 17953 (1994).
50. **G. Kresse and D. Joubert**: From ultrasoft pseudopotentials to the projector augmented-wave method. *Phys. Rev. B* **59**, 1758 (1999).
51. **J.P. Perdew, K. Burke, and M. Ernzerhof**: Generalized gradient approximation made simple. *Phys. Rev. Lett.* **77**, 3865 (1996).
52. **M. Methfessel and A.T. Paxton**: High-precision sampling for Brillouin-zone integration in metals. *Phys. Rev. B* **40**, 3616 (1989).
53. **H.J. Monkhorst and J.D. Pack**: Special points for Brillouin-zone integrations. *Phys. Rev. B* **13**, 5188 (1976).
54. **C. Freysoldt and J. Neugebauer**: First-principles calculations for charged defects at surfaces, interfaces, and two-dimensional materials in the presence of electric fields. *Phys. Rev. B* **97**, 205425 (2018).

https://doi.org/10.1557/jmr.2019.404 Published online by Cambridge University Press

© Materials Research Society 2020